Effect of hybrid industrial and recycled steel fibres on static and dynamic mechanical properties of ultra-high performance concrete

Hui Zhong [a], Meng Chen [b], Mingzhong Zhang [a,*]

[a] *Department of Civil, Environmental and Geomatic Engineering, University College London, London WC1E 6BT, UK*

[b] *School of Resources and Civil Engineering, Northeastern University, Shenyang 110819, China*

Abstract: Employing recycled tyre steel (RTS) fibres to replace industrial steel (IS) fibres in ultra-high performance concrete (UHPC) can improve its cost-effectiveness and sustainability. However, the lack of research on dynamic properties of such sustainable UHPC would hinder its application in concrete structures such as protective and defence structures which may experience different dynamic loadings. This paper experimentally investigates the effect of various RTS fibre replacement levels (0.5-2.0% by volume) on the flowability and quasi-static compressive, flexural and tensile strengths of UHPC as well as the dynamic splitting tensile behaviour under various strain rates (4.5-6.5 s^{-1}). The conventional UHPC with 2.0% IS fibre was prepared as the reference. Results indicate that the flowability of UHPC containing RTS fibres is about 5-11% higher than that of reference UHPC. Rising the RTS fibre replacement level up to 1.0% increases the compressive, flexural and tensile strengths while after which, the strengths drop. The dynamic splitting tensile behaviour of all UHPC specimens is sensitive to strain rate in terms of failure pattern, dynamic splitting tensile strength, dynamic increase factor and energy absorption capacity. Using 0.5% RTS fibre to substitute IS fibre can bring the best synergy, leading to the highest dynamic splitting tensile properties of UHPC at a strain rate of approximately 4.5-6.5 s^{-1}. The material cost, embodied carbon and embodied energy of UHPC are reduced by 9-57% in the presence of RTS fibres. The optimal RTS fibre replacement dosage for UHPC is 0.5% considering static mechanical properties, dynamic splitting tensile behaviour, material cost and environmental impact.

Keywords: High performance cementitious composites; Fibre reinforced concrete; Recycled fibre; Split Hopkinson pressure bar; Engineering properties; Sustainability

1. Introduction

Ultra-high performance concrete (UHPC) exhibiting extraordinary mechanical properties (e.g., ≥ 150 MPa in compressive strength [1]) and durability has been developed in the mid-1990s [2], which is designed by the tight particle packing of solid materials and adopting a very low water-to-binder ratio (< 0.2) [3]. Besides, sufficient chemical additives and a high volume fraction of steel fibres (≥ 2.0%) are needed during the mix design of UHPC [1]. Given the superior engineering properties of UHPC, it has been applied in various structural applications including long-span bridges and defence

* Corresponding author. E-mail address: mingzhong.zhang@ucl.ac.uk (M. Zhang)

facilities [4, 5]. For instance, UHPC has been adopted to develop a new desk-to-girder connection for concrete girder bridges [6]. However, the high cost and environmental impact associated with the commonly used industrial steel (IS) fibres in UHPC would hinder its large-scale application as well as the sustainable development of construction industry. For instance, the cost of UHPC with 1.5% (by volume) IS fibre is about 5-6 times higher than that of conventional concrete [7], and approximately 1.9 tonnes of CO_2 are emitted per tonne of IS fibre generated [8]. Therefore, finding other sustainable fibres with lower costs to replace IS fibres in UHPC is vital. In recent years, many efforts have been made towards this target and using recycled fibres from end-of-life tyres to substitute IS fibres is a promising option.

About 1500 million waste tyres are generated every year and most of them are disposed of without any treatment, intensifying the burden on landfilled regions and increasing contamination areas [9, 10]. One of the solutions to address these concerns is to recycle the usable materials from the waste tyres such as crumb rubber, steel wires and textile fibres and adopt them as the ingredients of construction materials. Further, the carbon footprint can be reduced as recycling waste tyres could avoid approximately 1520 tonnes of CO_2 emissions every year [11]. The steel fibres recycled from the waste tyres are known as recycled tyre steel (RTS) fibres in literature, which can be mainly recovered through the mechanical recycling process [12]. In the past decade, many studies explored the feasibility of partial or full replacement of IS fibres with RTS fibres in fibre reinforced concrete that can achieve a compressive strength of 30-80 MPa [13-25]. It was indicated that under the same fibre content (0.25-2.0%), the flexural post-cracking behaviour, dynamic compressive properties and chloride-induced corrosion resistance of RTS fibre reinforced concrete were comparable to those of composites with IS fibres [13, 14, 16-18], while it was also reported that the RTS fibre content should be twice more than that of IS fibre to achieve comparable engineering properties for RTS and IS fibre reinforced concrete, due to the irregular dimension of RTS fibres [15]. In addition, partially replacing IS fibres with RTS fibres can create a synergistic effect to exhibit a 39% higher post-cracking residual strength [25] and similar tensile strength and flexural behaviour as compared with mono-IS fibre reinforced concrete when the replacement ratio was lower than 50% [23, 24]. Most hybrid mixtures surpassed composites with RTS fibres only in terms of various properties [23, 24].

To date, the effect of RTS fibre on the fresh and hardened properties of UHPC such as workability, compressive strength, flexural behaviour and shear performance has been rarely investigated [8, 26-28]. The strength of UHPC can be affected by the cleanness and length of RTS fibre, where the mixture had a lower strength if the used RTS fibres contained many rubber particles and impurities or the length of most RTS fibres was less than 9 mm. Increasing the RTS fibre dosage can consistently improve the compressive strength, flexural strength, shear strength and elastic modulus of UHPC but weakened the workability. Nevertheless, these studies did not compare the performance between RTS

fibre reinforced UHPC and UHPC with IS fibres, which were mainly focused on the static mechanical properties while the dynamic properties have not been explored. It is worth noting that UHPC is promising to be applied in structures that may be subjected to dynamic loadings such as protective and military applications [29].

Until now, many studies have explored the dynamic mechanical behaviour of UHPC especially dynamic compressive properties (e.g., [30-33]). It should be mentioned that concrete structures may fail more easily under dynamic tension [34, 35] and therefore, a growing number of studies have been focused on the dynamic tensile behaviour of UHPC [36-42]. Most of them found that similar to normal concrete, the tensile properties of UHPC were significantly sensitive to the strain rate. For instance, the average uniaxial tensile strength of UHPC was improved by 45.49% when the strain rate raised from 0.2 s^{-1} to 5 s^{-1} [37]. Under the same fibre dosage, the effects of different nanomaterials including nano-$CaCO_3$, nano-SiO_2, nano-TiO_2 and nano-Al_2O_3 on the dynamic tensile behaviour of UHPC were not significant, whereas increasing their dosages can enhance the strength of UHPC [38]. The dynamic spalling strength of UHPC went up with the rising dosage of either straight IS fibre or hooked-end IS fibre and the straight IS fibre had a slightly better effect on enhancing the dynamic spalling strength than hooked-end IS fibre when the fibre volume fraction was 1.0% and the strain rate was greater than 60 s^{-1} [39]. Similarly, it was reported that the presence of IS fibres prevented the splitting failure of UHPC samples, maintaining their structural integrity [42]. Nevertheless, most of these previous studies only focused on the dynamic tensile behaviour of UHPC with IS fibres and to the authors' best knowledge, the research on the effect of fibre with lower cost and higher sustainability on the tensile behaviour of UHPC under various strain rates is still lacking. As mentioned previously, incorporating RTS fibres into UHPC has a great potential to improve its cost-effectiveness and sustainability whereas the effect of RTS fibre on the quasi-static mechanical properties and dynamic tensile behaviour of UHPC is still unclear, which can limit its widespread application. To ensure the future safe design of concrete structures containing RTS fibre reinforced UHPC, it is essential to get a comprehensive understanding of the effects of RTS fibre content and strain rate on the dynamic tensile behaviour of UHPC. In addition, both direct and indirect tension approaches have been applied to characterise the dynamic tensile behaviour of UHPC [41], while using the latter one through split Hopkinson pressure bar (SHPB) can offer many benefits over the former one such as better achievement of dynamic stress equilibrium and easier testing preparation and setup [36, 43, 44]. Hence, it was selected for characterising the dynamic tensile behaviour of UHPC in this study.

The main purpose of this study is to comprehensively investigate the effects of partial and full replacement of IS fibres with RTS fibres on the quasi-static and dynamic mechanical properties of UHPC, at a controlled total fibre volume fraction of 2.0%. Four replacement ratios including 25%,

50%, 75% and 100% were used. A series of tests were first conducted to measure the workability as well as quasi-static compressive, flexural and tensile strengths of all UHPC mixtures. A 100-mm SHPB device was employed to characterise the dynamic splitting tensile properties of UHPC mixes including failure pattern, stress-time response, dynamic splitting tensile strength, dynamic increase factor (DIF) and energy absorption capacity. Lastly, an optimal mixture for hybrid fibre reinforced UHPC was proposed considering material cost and environmental impact as well as quasi-static and dynamic mechanical properties.

2. Experimental program

2.1. Raw materials

P.I. 52.5 Portland cement and silica fume were used as the binders, the chemical compositions and particle size distribution of which are shown in Table 1 and Fig. 1, respectively. Quartz sand with a size range of 500-600 μm was adopted as fine aggregate and a polycarboxylate-based superplasticiser was used to adjust the workability of UHPC mixtures. Fig. 2 presents some photos of the binders and sand used in this study.

Table 1 Chemical compositions (wt.%) of cement and silica fume.

Oxide	CaO	SiO_2	Al_2O_3	Fe_2O_3	SO_3	MgO	K_2O	Loss on ignition
Cement	63.03	20.19	5.11	2.11	1.19	1.72	0.32	2.14
Silica fume	-	94.77	0.35	-	-	-	-	0.66

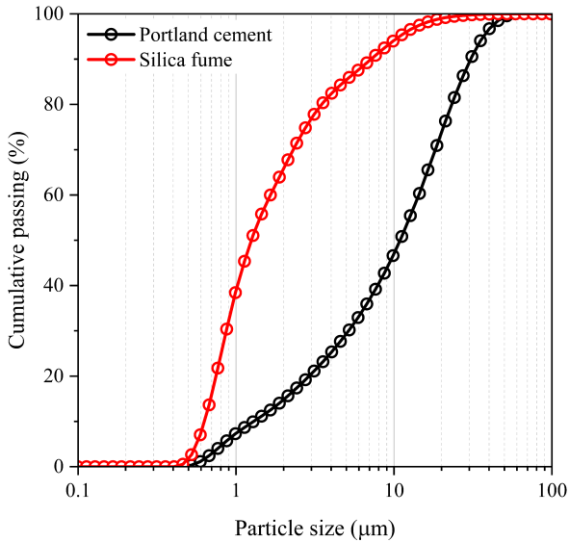

Fig. 1. Particle size distribution of Portland cement and silica fume.

Fig. 2. Photos of Portland cement, silica fume, quartz sand and industrial steel (IS) fibres.

Straight IS (Fig. 2) and RTS fibres were adopted to reinforce the matrix of UHPC, the properties of which are listed in Table 2. The length of the as-received RTS fibres was not uniform and ranges from 2 mm to 27 mm. As reported by existing literature [8, 30, 45, 46], the length of steel fibre can considerably affect the fresh and hardened properties of UHPC. Thus, an optimal length distribution range for RTS fibres should be determined first by evaluating the effect of RTS fibres with various length ranges on the fresh properties and quasi-static mechanical properties of UHPC. To divide the as-received RTS fibres into three groups with different length distributions (i.e., short, medium and long), a screening process employing different sieves and a vibration table was performed, the schematic illustration of which is given in Fig. 3. Three various types of RTS fibres were obtained named 'RTS-L', 'RTS-M' and 'RTS-S', respectively, and the corresponding length distribution was characterised based on a sample size of 500. Fig. 4 displays the length distribution of these fibres and as-received RTS fibres. Around 79% of RTS-S fibres have a length of 4-9 mm, while about 68% of RTS-M fibres have a length between 9 mm and 16 mm. RTS-L is the longest one, with more than 90% of them having a length of 16-24 mm. Based on the preliminary results, it can be found that UHPC with RTS-M outperformed other UHPC mixtures in terms of static compressive, flexural and tensile strengths (about 2-28% higher). Although the static mechanical properties of UHPC containing RTS-M were poorer than that with IS fibres (around 4-22% lower), its workability was about 9% higher. Therefore, RTS-M was selected and used in this study to replace IS fibres partially and fully.

Table 2 Properties of IS and as-received RTS fibres.

Fibre	Length (mm)	Diameter (μm)	Tensile strength (MPa)	Elastic modulus (GPa)
IS	13	200	2000	220
RTS	2-27	220	2165	200

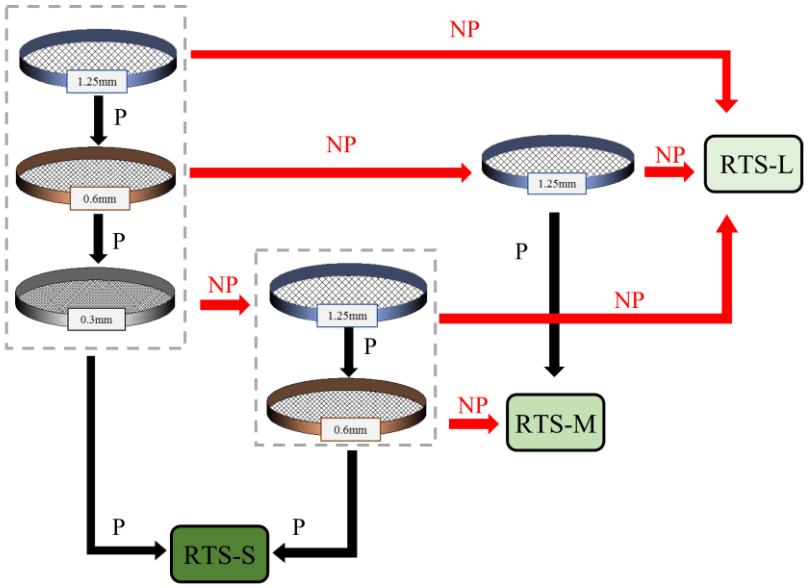

Fig. 3. Schematic illustration of screening process for RTS fibres (note: P = Pass, NP = Not Pass).

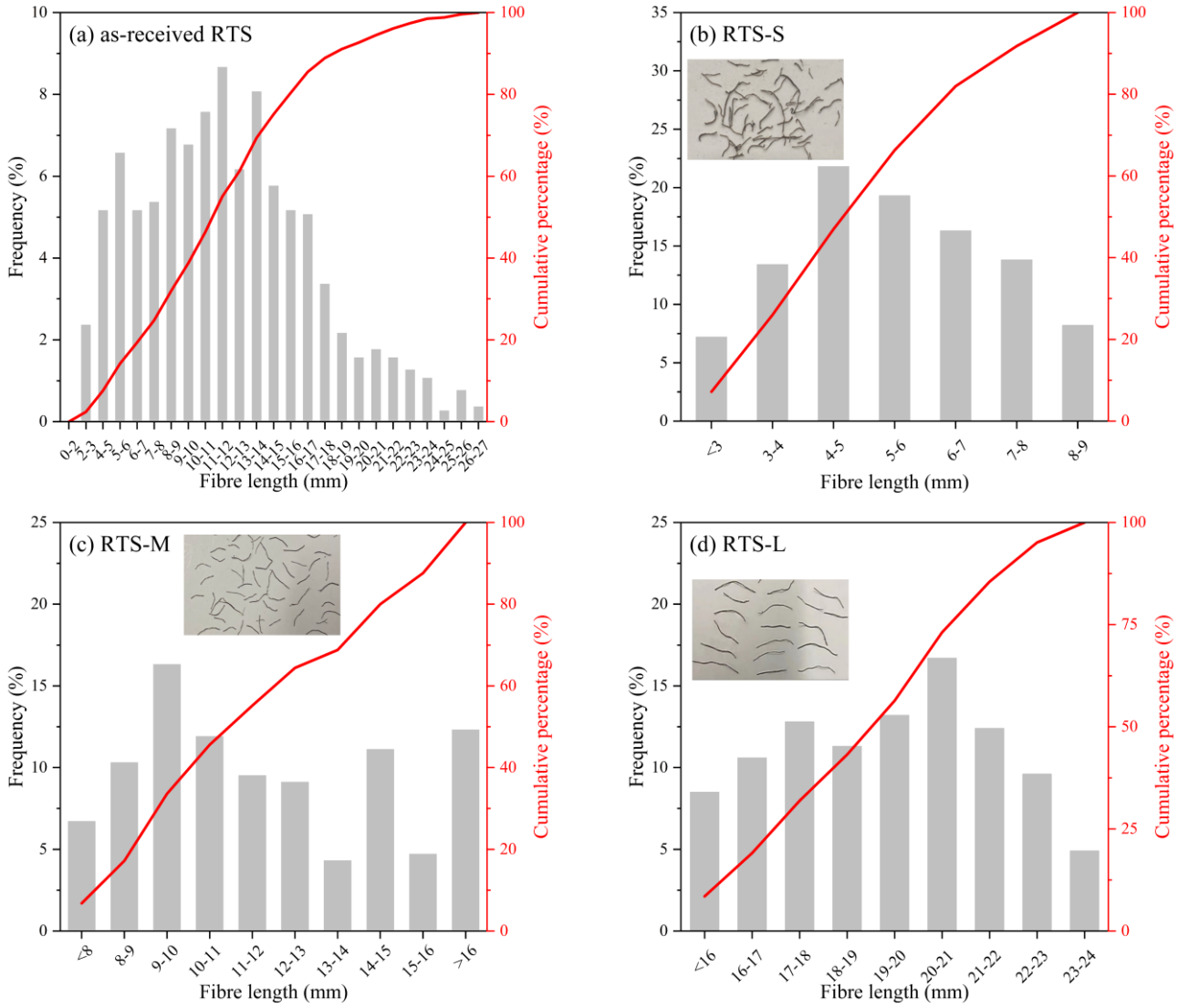

Fig. 4. Length distribution of (a) as-received RTS fibres, (b) RTS-S, (c) RTS-M, and (d) RTS-L.

2.2. Mix proportions

Table 3 shows the mix proportions of all UHPC mixtures, where the water-to-binder ratio was selected as 0.18 and the superplasticiser dosage was 2.1% of the total binder weight to ensure acceptable workability for all mixes. The weight ratios of cement, silica fume and quartz sand were 1.0:0.25:1.4. The matrix was reinforced with either IS fibres, RTS fibres or a combination of IS and RTS fibres. Regarding the meaning of mix ID, I2.0 means the mix with 2.0% IS fibre while I1.5R.05 denotes the mixture containing 1.5% IS fibre and 0.5% RTS fibre.

Table 3 Mix proportions of UHPC used in this study.

Mix ID	By weight (kg/m^3)					By volume (%)	
	Cement	Silica fume	Quartz sand	Water	Superplasticiser	IS fibre	RTS fibre
I2.0						2.0	0
I1.5R0.5	788	200	1100	182	21	1.5	0.5
I1.0R1.0						1.0	1.0

I0.5R1.5	0.5	1.5
R2.0	0	2.0

2.3. Specimen preparation

The following mixing procedure was employed for all investigated UHPC mixtures: (1) all powders and sand were dry mixed for 3 min; (2) steel fibres were added and mixed for 2 min; (3) half of the mixing water and all superplasticisers were added and mixed for 3 min; (4) the remaining water was added and mixed for 2 min, followed by a 3 min high-speed mixing. After mixing, all fresh mixtures were poured into moulds of different sizes. All samples were de-moulded after 24 h and then cured in a standard curing room (20 ± 2 °C and 95% relative humidity) for 28 d.

2.4. Testing methods

2.4.1. Flowability test

The flow table test was conducted to estimate the workability of UHPC mixtures as per ASTM C1437-15 [47]. Upon the completion of mixing, the mixtures were first poured into a mini-slump cone, followed by elevating the cone and striking the flow table 25 times in 15 s. Then, the spread diameters in two directions were measured and the mean value was adopted. The test setup is illustrated in Fig. 5. The above process was repeated three times for each mixture.

Fig. 5. Experimental setup of flowability test.

2.4.2. Flexural and compressive tests

The flexural strength of UHPC specimens measuring 40 mm × 40 mm × 160 mm ($b \times h \times l$) was determined by a four-point bending test according to EN196-1 [48] and its test setup is shown in Fig. 6. The flexural strength (f_f) of test specimens can be calculated as:

$$f_f = \frac{F_{max} L}{bh^2} \quad (1)$$

where F_{max} is the maximum flexural load recorded by the testing machine, and L is the loading span (i.e., 100 mm).

After four-point bending test, two broken parts of the specimen were used for compressive test. The compressive strength of test specimens was determined by dividing the maximum compressive

load by the loading area. For each mixture, three samples were tested to determine the average flexural strength while six samples were tested to obtain the average compressive strength.

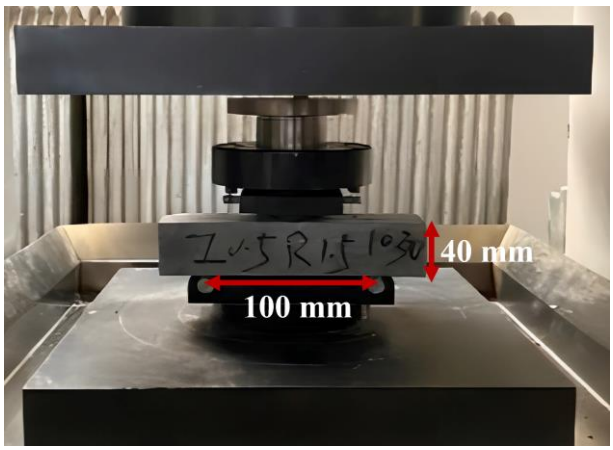

Fig. 6. Experimental setup of flexural test.

2.4.3. Uniaxial direct tensile test

For each mixture, the uniaxial direct tensile test was performed on three dog-bone shaped specimens (see Fig. 7a) using a universal tensile testing machine [49], as demonstrated in Fig. 7b. During the test, a constant displacement-controlled loading rate of 0.5 mm/min was utilised. The results were only valid when the final crack appeared within the central region (dark green) of the specimen.

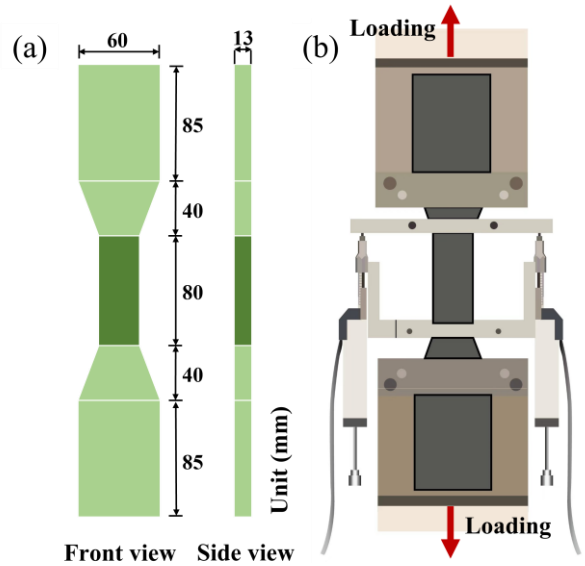

Fig. 7. Schematic diagram of (a) dog-bone shaped specimen and (b) experimental setup of uniaxial direct tensile test.

2.4.4. Quasi-static splitting tensile test

The quasi-static splitting tensile test was carried out on three UHPC specimens measuring ∅100 mm × 50 mm for each mixture, as displayed in Fig. 8, where two plywood pieces were placed between the test sample and the loading plates to help attain a uniform stress distribution [52]. The used sample size was kept consistent with that for the dynamic splitting tension test to attain reliable DIF values

[50, 51]. After the test began, a vertical load was applied along the diameter of the test sample with a constant loading rate of 0.5 mm/min.

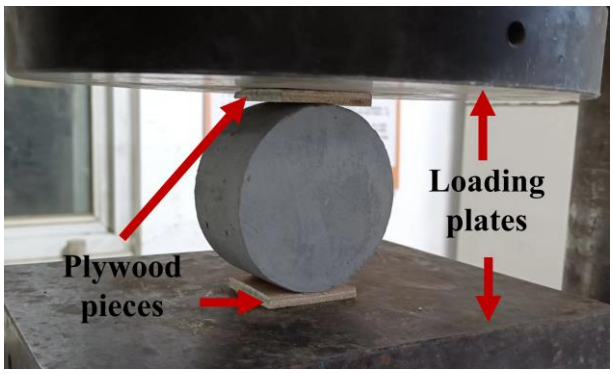

Fig. 8. Experimental setup of quasi-static splitting tensile test.

2.4.5. Dynamic splitting tensile test

A 100-mm SHPB testing apparatus was employed to evaluate the dynamic splitting tensile behaviour of UHPC specimens, the schematic illustration and photograph of which are given in Fig. 9. The striker, incident, transmission and absorbing bars are all made of high-strength steel materials and their lengths are 600 mm, 5000 mm, 3500 mm and 1200 mm, respectively. The test specimen (Ø100 mm × 50 mm) was placed between the incident bar and the transmission bar prior to the impact test. Once the striker bar impacted the left end of the incident bar, an incident wave was generated and propagated towards the test sample. When the incident wave reached the sample, part of the wave was reflected and the remaining continued to propagate along the transmission bar. Based on previous studies [51, 53, 54], a rubber pulse shaper with diameter of 50 mm and thickness of 2 mm was placed at the left end of the incident bar to promote the dynamic stress equilibrium. Fig. 10 shows a typical check of dynamic stress equilibrium, indicating that the transmission stress was close to the sum of the incident stress and reflected stress. It suggests that the test specimen was in a state of stress equilibrium under dynamic loading [55]. The strain gauges mounted on the incident and transmission bars were used to measure the history of incident strain ($\varepsilon_i(t)$), reflected strain ($\varepsilon_r(t)$) and transmission strain ($\varepsilon_t(t)$). The history of dynamic splitting tensile stress ($\sigma_{dt}(t)$) was calculated as follows [54]:

$$\begin{cases} \sigma_{dt}(t) = \dfrac{2F_{dt}(t)}{\pi D_s L_s} \\ F_{dt}(t) = E_b A_b \varepsilon_t(t) \end{cases} \tag{2}$$

where $F_{dt}(t)$ is the history of dynamic splitting tensile force, E_b and A_b denote the elastic modulus and cross-sectional area of the SHPB bar, respectively, and D_s and L_s represent the diameter and length of the test specimen, respectively.

The strain rate for each test ($\dot{\varepsilon}$) and the energy absorption capacity of UHPC specimens (W_{dt}) can be derived as follows [56-58]:

$$\begin{cases} \dot{\varepsilon} = \dfrac{f_{dt}}{t_0 E_s} \\ W_{dt} = E_b A_b C_b \displaystyle\int_0^t (\varepsilon_i^2(t) - \varepsilon_r^2(t) - \varepsilon_t^2(t))\, dt \end{cases} \tag{3}$$

where f_{dt} is the dynamic splitting tensile strength, t_0 denotes the time required to achieve the peak of transmission stress, E_s represent the elastic modulus of the test sample, and C_b is the longitudinal wave velocity of the SHPB bar.

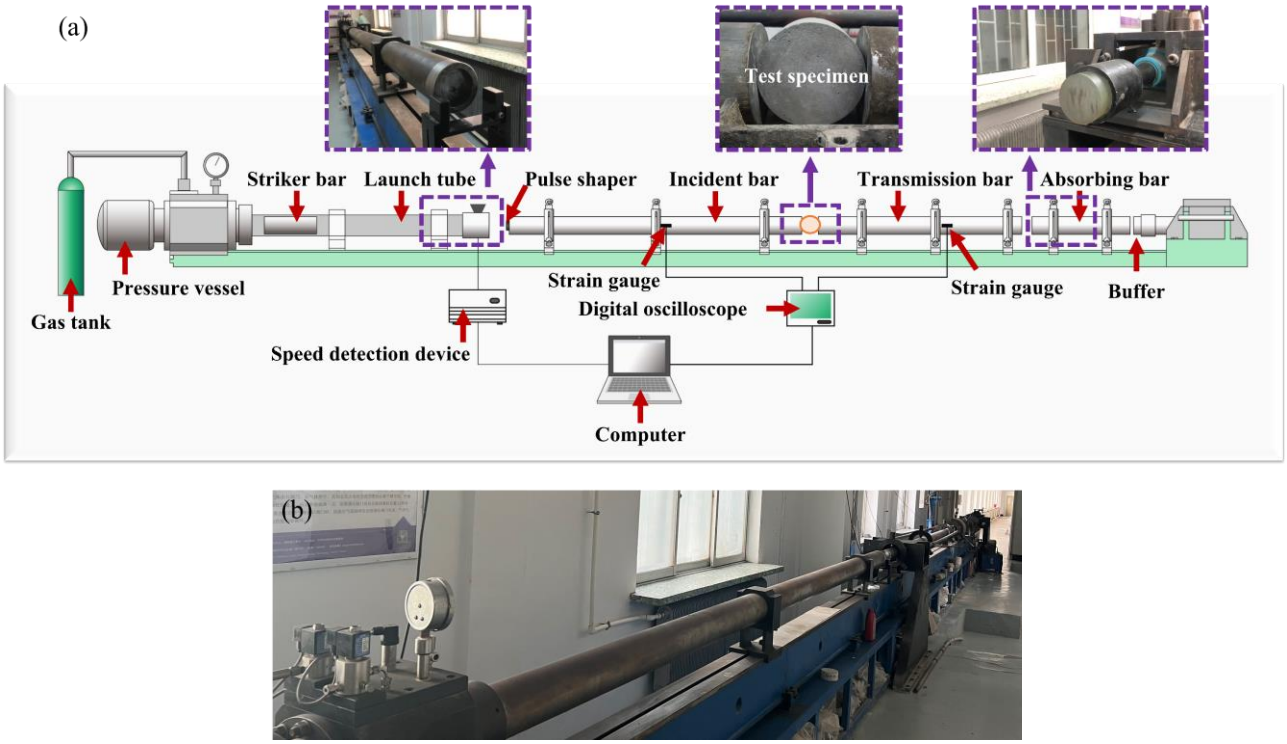

Fig. 9. SHPB device: (a) schematic illustration, and (b) photo of the real device.

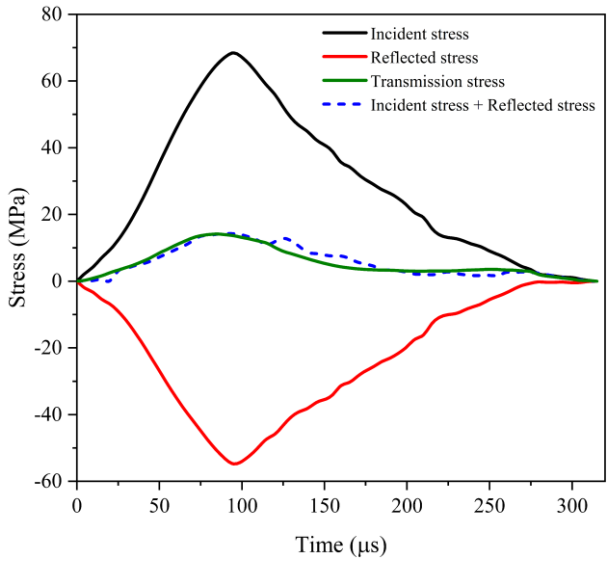

Fig. 10. An example of checking dynmaic stress equilibrium.

3. Results and discussion

3.1. Flowability

Fig. 11 illustrates the measured slump flow of all UHPC mixtures, ranging from 226 mm to 251 mm. The flowability of UHPC containing RTS fibres was about 5-11% higher than that of I2.0, which can be ascribed to the smaller aspect ratio of RTS fibres. IS fibres have an aspect ratio of 65, while around 69% of the used RTS fibres have an aspect ratio smaller than 65 (Fig. 4c). Fibres with higher aspect ratios have larger surface areas and may absorb more water, leading to reduced workability [59-61]. In IS fibre reinforced UHPC, the flowability tends to be lower when the used IS fibres have deformed shapes as compared to UHPC with straight IS fibres [62, 63]. Herein, although some RTS fibres are not straight (Fig. 4c), increasing the RTS fibre dosage in hybrid fibre reinforced UHPC still improved the workability. This can be attributed to the mutual effect between hybrid fibres, which can restrict each other's rotation to prevent the fibres from orienting perpendicular to the flow direction [64]. The largest shear resistance can be induced when most fibres are distributed perpendicular to the flow direction of the matrix. Similar findings were reported in other studies [30, 64] that using hybrid long and short IS fibres can result in better workability for UHPC as opposed to the mixture with solely long IS fibres. For instance, when the short IS fibre volume fraction was between 0.5% and 1.5%, the flowability of UHPC was around 3-7% larger than that of UHPC with 2.0% long IS fibre [30]. As the RTS fibre replacement dosage increased, the positive effect of RTS fibre on the flowability of UHPC gradually minimised. This can be evidenced by the similar slump flow values of I1.0R1.0 (244 ± 4.4 mm), I0.5R1.5 (251 ± 5.3 mm) and R2.0 (246 ± 4.0 mm).

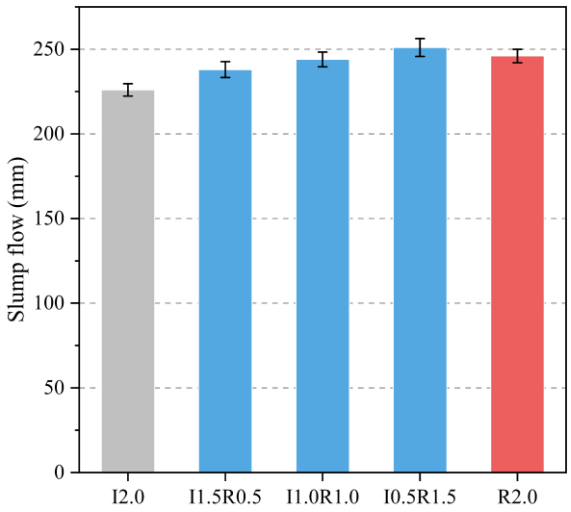

Fig. 11. Flowability of UHPC mixtures.

3.2. Quasi-static compressive and flexural strengths

The quasi-static compressive strength of UHPC is presented in Fig. 12a, revealing that irrespective of reinforcing fibre type and content, all mixes had a compressive strength of larger than 168 MPa. I1.5R0.5 achieved the highest compressive strength of 186 MPa, while R2.0 exhibited the lowest one. As the RTS fibre replacement level increased, the compressive strength of UHPC was raised first,

followed by a decline. The compressive strengths of I1.5R0.5 and I1.0R1.0 were about 2% and 6% greater than that of I2.0, which can be explained by the fact that: (1) the compactness of these hybrid fibre reinforced UHPC mixtures is better because of the higher flowability; (2) a synergistic effect of hybrid fibres is generated to control the cracks; (3) some RTS fibres with longer lengths (≥ 13 mm) can better restrain the crack propagation compared to IS fibres; and (4) RTS fibres with deformed shapes can offer additional mechanical anchorage to improve the bonding with matrix [60]. When the RTS fibre content went up to 1.5% and 2.0%, the compressive strength of resultant composites was 3-4% lower than that with IS fibres only, primarily due to the reduced efficiency in restraining the cracks when less long fibres were present. Additionally, some RTS fibres may be damaged during the recycling process, raising the possibility of weakening the mechanical performance of UHPC [15, 65]. Previous studies [30, 64, 66, 67] reported similar results that the short fibre replacement content should be limited to ensure acceptable compressive strength. For instance, the 28-d compressive strengths of UHPC containing 0.5-1.0% short IS fibres were about 8-14% smaller than that of UHPC incorporating 0.25% short IS fibres [64]. Similarly, the compressive strength of UHPC with 1.5% long IS fibre and 1.0% short IS fibre was around 12% lower than that with 2.5% long IS fibre [67].

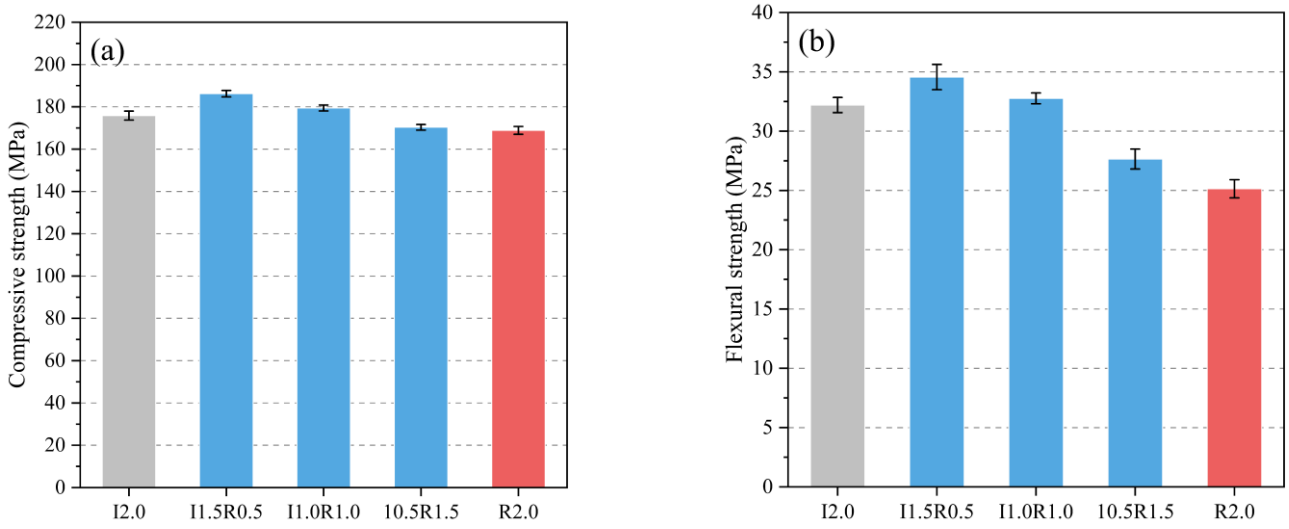

Fig. 12. Effects of IS and RTS fibres on (a) compressive strength and (b) flexural strength of UHPC.

Fig. 12b presents the flexural strength of UHPC with different fibre types, where the changing trend of flexural strength with RTS fibre content was consistent with that of compressive strength. I1.5R0.5 attained the largest flexural strength of 34.6 MPa, which was 7.33% and 37.49% higher than that of I2.0 and R2.0, respectively. This can be mainly ascribed to the synergistic effect of IS and RTS fibres in controlling the cracks at two scales, where short RTS fibres can control the initiation and growth of micro-cracks while IS fibres and long RTS fibres tend to bridge the cracks with larger sizes. Previous studies revealed a similar synergistic effect when hybridising long and short steel fibres in UHPC, where the flexural strength of UHPC containing 1.5% long IS fibre and 0.5% short

IS fibre was better than that with 2.0% long IS fibre [30, 64, 67]. Unlike compressive strength, the reduction degree in flexural strength was larger when more RTS fibres were present. For instance, the flexural strength of I0.5R1.5 was around 14% lower than that of I2.0, while only a 3% drop can be observed in compressive strength, implying that the fibre bridging effect plays a more dominant role in flexural behaviour [68]. Hence, to ensure an acceptable flexural behaviour for hybrid fibre reinforced UHPC, the dosage of RTS fibre should be limited.

3.3. Quasi-static tensile strength

Fig. 13 illustrates the uniaxial tensile and splitting tensile strengths of UHPC specimens, indicating that the changing trends of them with RTS fibre dosage were similar to those of compressive and flexural strengths. Regardless of reinforcing fibre, the splitting tensile strengths of all mixtures were about 59-69% higher than their uniaxial tensile strengths, due to the disparate fracture processes. Whist the splitting tension, the tangential stress would surpass the uniaxial tensile strength, leading to the final failure [43]. Fibre bridging behaviour plays an important role during both uniaxial and splitting tensile loadings, and some images showing the cracking interfaces are given in Fig. 14. Both pulled out and ruptured fibres can be observed in UHPC with 2.0% IS fibre (Fig. 14a). Fibre pull-out tends to improve the overall tensile behaviour, while fibre rupture may lead to crack localisation which can appear due to the hydrophilic surface feature of IS fibres or when the fibre inclination angle exceeds a certain degree [68, 69]. As seen in Fig. 14b, there exists a synergistic fibre effect in hybrid fibre reinforced UHPC, suggesting that when the incorporated RTS content is appropriate (e.g., 0.5%), the short RTS fibres can effectively bridge the micro-cracks, while IS fibres and long RTS fibres start their actions when the micro-cracks propagate into macro-cracks. The coefficient of variation values (i.e., ratio of standard deviation to mean) of uniaxial tensile strengths ranged from 4.3% to 7.5%, significantly greater than those of splitting tensile strengths (1.4-2.9%), which can be strongly associated with the fibre dispersion inside UHPC. Only the fibre distribution and orientation along the diameter of the test specimen are critical to its splitting tensile strength as the major splitting crack appears along the centre of the test specimen. While under the uniaxial tensile loading, a crack normally is initiated from the largest flaw inside the test specimen and then propagates along the weakest zone [70]. If the number of effective fibres (i.e., fibres perpendicular to the crack plane and with smaller inclination angles) across the crack interface is lower, the test specimen would fail quickly resulting in lower ultimate strength. Thus, the variability of uniaxial tensile strength tends to be higher than that of splitting tensile strength due to the uncertain location of the crack appearance and the effective fibre number crossing the crack interface. This phenomenon was also captured by other studies [71, 72].

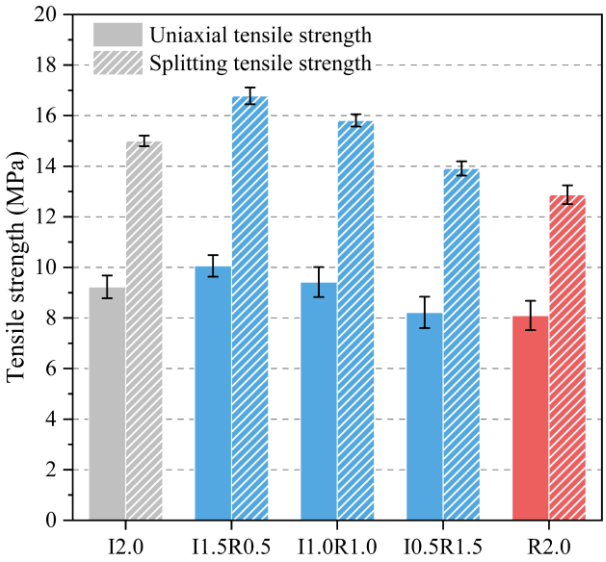

Fig. 13. Effects of IS and RTS fibres on uniaxial tensile and splitting tensile strengths of UHPC.

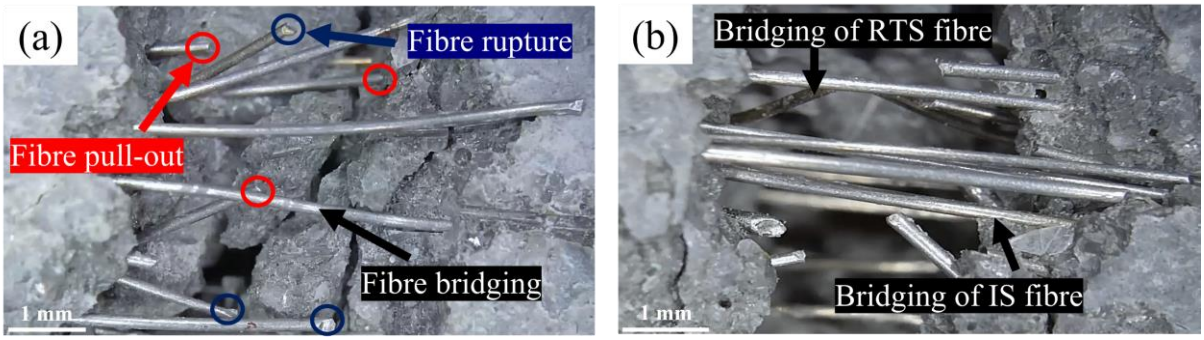

Fig. 14. Fibre conditions across the cracking interface of (a) mono-IS fibre reinforced UHPC and (b) hybrid fibre reinforced UHPC.

3.4. Dynamic splitting tensile properties

3.4.1. Failure pattern

Fig. 15 displays the failure patterns of all UHPC specimens under various strain rates. The major cracks of all specimens passed through their centre, confirming the validity of the results. All mixtures were sensitive to strain rate, where the damage degree (e.g., crack width) went up with the increasing strain rate. This can be attributed to the increased crack velocity, accelerating the crack initiation and propagation and thus weakening the fibre bridging behaviour. A similar phenomenon was captured by a previous study on UHPC [42], where increasing the strain rate induced more cracks at the interface between the test specimen and bars. At a strain rate of 6.53-6.68 s^{-1}, most specimens exhibited triangular damage near the loading ends, possibly due to the increased stress concentration at the loading points [51].

Replacing IS fibres with a certain content of RTS fibres can mitigate the damage loss of UHPC under a similar strain rate, while the presence of excessive RTS fibres can intensify the damage. For instance, at a strain rate of 5.31-5.48 s^{-1}, the crack width of I1.5R0.5 was smaller than that of I2.0, and many bridging fibres can be identified at the crack interface. By contrast, the specimens of

I0.5R1.5 and R2.0 were split into two halves with fewer bridging fibres across the interface. The causing reasons are similar to those explained for quasi-static mechanical properties. In addition, employing a suitable dosage of RTS fibre to substitute IS fibre can lead to a favourable fibre orientation for UHPC, where more fibres can be distributed perpendicular to the loading direction. The positive effect of utilising hybrid fibre reinforcement to resist the dynamic failure of UHPC was also found in Ref. [30], where UHPC with 2.0% long IS fibres presented relatively large and round broken fragments after dynamic compression with a strain rate of around 115 s^{-1}, while the sizes of broken fragments for UHPC containing both long and short IS fibres were more balanced.

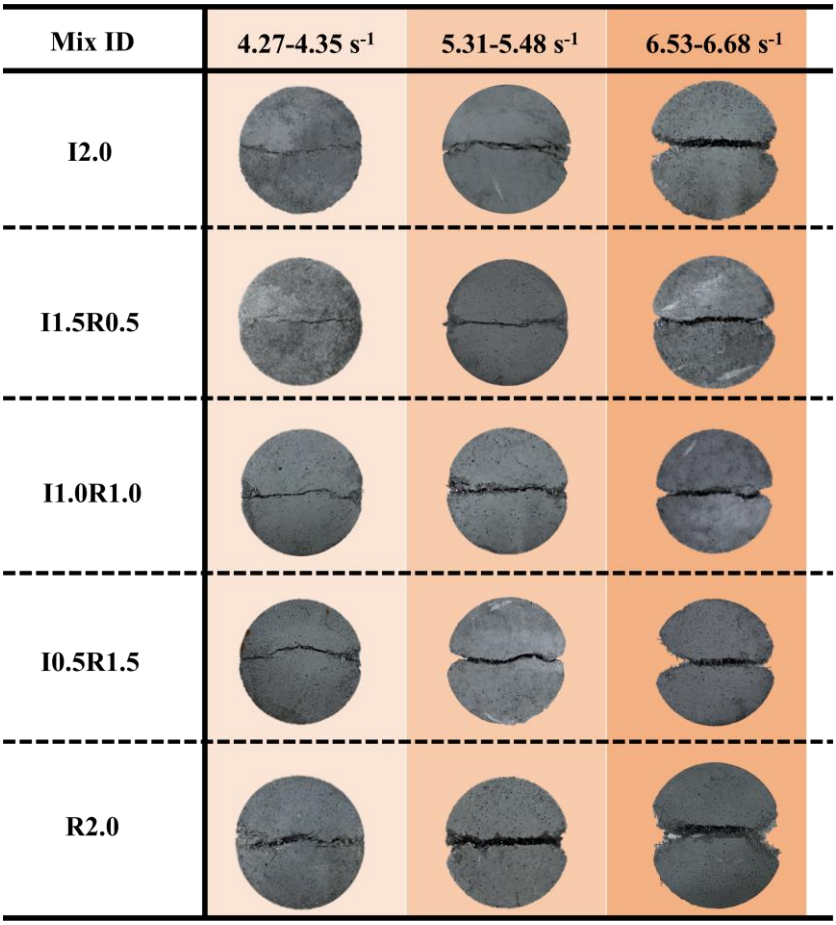

Fig. 15. Effects of strain rate and fibre on failure pattern of UHPC.

3.4.2. History of dynamic splitting tensile stress

Fig. 16 demonstrates the history of dynamic splitting tensile stress at different strain rates, indicating that all curves are comparable in shape and contain ascending and descending regions. In the first region, the dynamic splitting tensile stress went up gradually and the first visible crack was initiated in the central portion of the specimen after reaching the elastic limit. Afterwards, the crack started propagating towards the loading ends but its width did not vary remarkably owing to the fibre bridging effect [42, 56, 71]. This phenomenon happened during the region between the elastic limit and the peak stress. Then, as the crack continued to propagate with the increasing crack width, the fibres were either pulled out or ruptured and the dynamic stress dropped. Some stress fluctuations can

be found in the descending stages of all mixtures, which can be associated with the rising contact area between the test specimen and the bars [42]. Similar fluctuations were noticed by other studies [42, 50, 73] when using steel fibres as reinforcement. As the strain rate raised, the slope of the elastic region for all UHPC specimens went up, consistent with the previous discussion on the increased crack velocity with the rising strain rate (Section 3.4.1). Changing the fibre type or dosage did not significantly alter the shape of the curve, while the peak stress (i.e., dynamic splitting tensile strength) and corresponding energy absorption capacity were disparate which will be further discussed in the following sections.

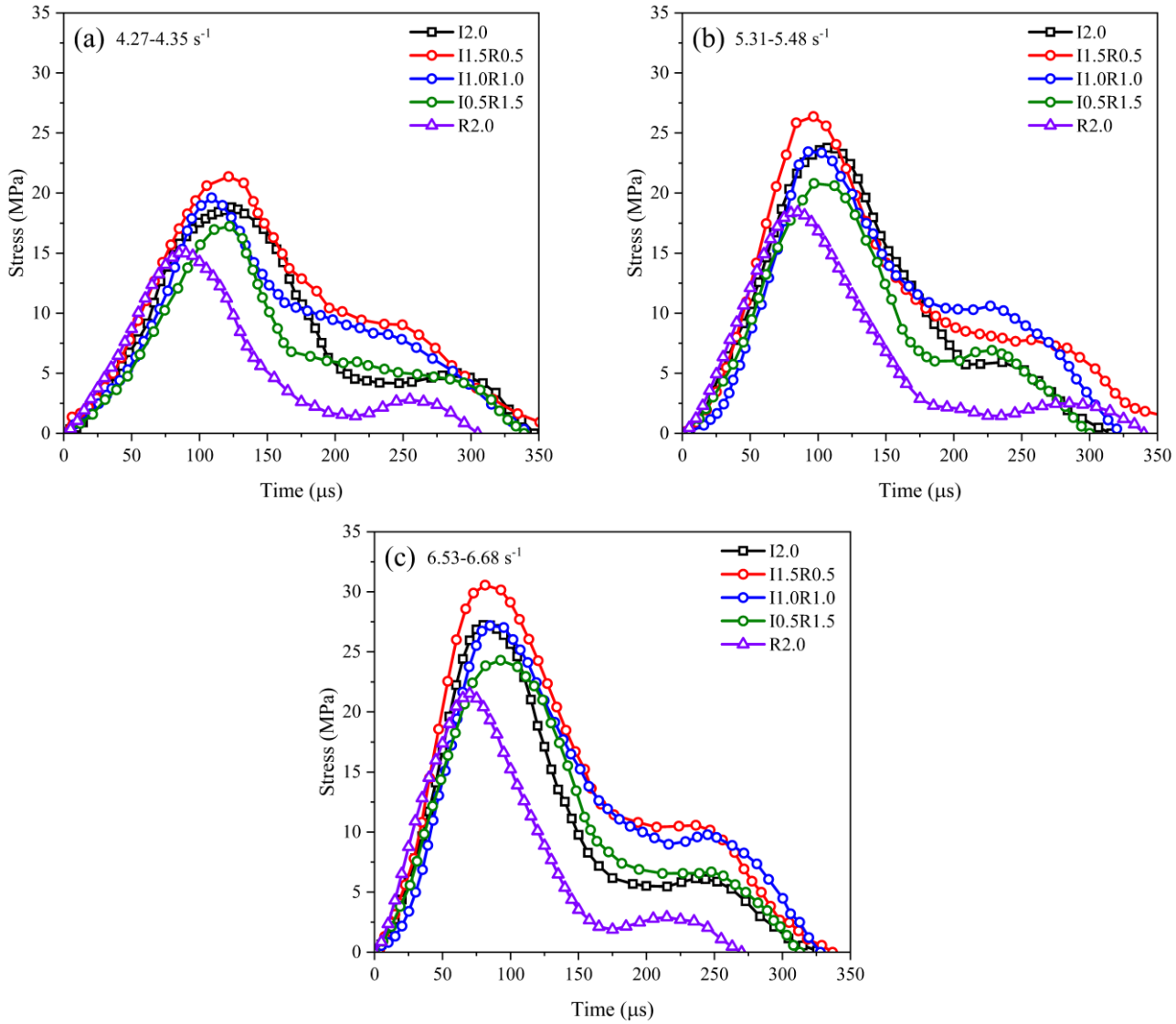

Fig. 16. Dynamic splitting tensile stress-time response of UHPC specimens at different strain rates.

3.4.3. Dynamic splitting tensile strength

Fig. 17 shows the effects of strain rate and fibre on the dynamic splitting tensile strength of UHPC. Like failure patterns, the dynamic splitting tensile strength was strain-rate dependent, which went up substantially with the rising strain rate. For instance, the dynamic splitting tensile strengths of I2.0, I1.5R0.5, I1.0R1.0, I0.5R1.5 and R2.0 were improved by 26.35%, 23.34%, 19.53%, 20.71% and

22.57%, respectively, when the strain rate changed from about 4.5 s^{-1} to 5.5 s^{-1}, which can be explained by the following reasons [42, 43, 50, 56, 74]: (1) the increased crack velocity can increase the rates of crack generation and propagation and more micro-cracks are formed beside the major crack, consuming more energy; (2) the presence of viscous liquid inside the specimen can resist the crack propagation and this resistance is proportional to the crack velocity; and (3) the lateral inertia effect, i.e., the lateral deformation of the test specimen under a high-speed impact loading (due to the Poisson's effect) is confined by the backward inertia force.

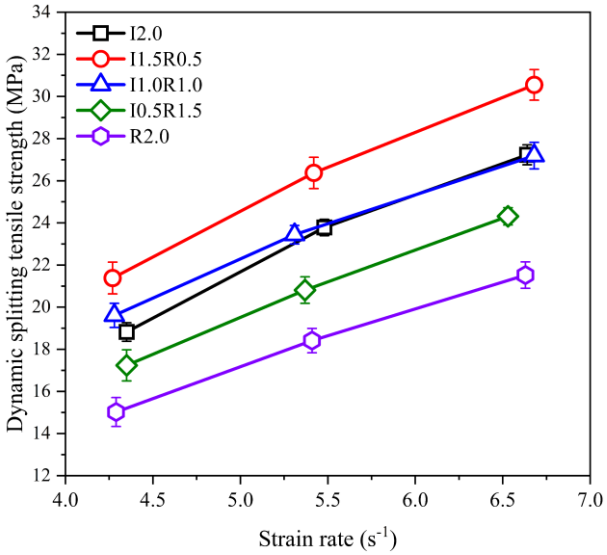

Fig. 17. Dynamic splitting tensile strength of UHPC at various strain rates.

Consistent with the results of quasi-static mechanical properties, I1.5R0.5 attained the highest dynamic splitting tensile strength at each test strain rate while R2.0 exhibited the lowest one. The dynamic splitting tensile strength of I1.5R0.5 was about 11-14% higher than that of I2.0, while I1.0R1.0 had comparable performance to I2.0 at various strain rates. Similar to the quasi-static loading, the synergistic effect of hybrid IS and RTS fibres contributed to the strength improvement and the better fibre orientation can intensify this effect. As aforementioned, some deformed RTS fibres can enhance the bonding with the matrix, which can be further increased with the increasing strain rate. However, the strain rate effect on the straight steel fibre was found to be insignificant [35]. Therefore, partially replacing straight IS fibres with mostly deformed RTS fibres can result in better dynamic splitting tensile strength as opposed to UHPC containing 2.0% IS fibre. When the RTS fibre replacement level reached 1.5% and 2.0%, the dynamic splitting tensile strengths of UHPC were found to be 8.40-12.49% and 20.19-22.58% lower than that of I2.0, which can be attributed to the reduced fibre bridging capacity as a result of the rising number of short or damaged RTS fibres. Similar findings were reported in previous studies on the dynamic compressive behaviour and drop hammer impact performance of UHPC [30, 67]. When the strain rate was between 114.8 s^{-1} and 195.8 s^{-1}, the dynamic compressive strength of hybrid fibre reinforced UHPC was 13.10-15.45% higher than that of mono-fibre reinforced UHPC [30]. In addition, the peak impact force of hybrid fibre

reinforced UHPC was 655.85 kN after the drop hammer loading, about 17% greater than that of UHPC with 2.0% long IS fibre [67].

3.4.4. Dynamic increase factor

DIF of UHPC here is defined as the ratio of dynamic splitting tensile strength to quasi-static tensile strength, which is regarded as a critical parameter for future structural design and numerical simulations [30]. Fig. 18a presents the DIF values of UHPC under a strain rate ranging from 4.27 s^{-1} to 6.68 s^{-1}, indicating that a consistent changing trend of DIF against strain rate with that of dynamic splitting tensile strength while their trends against the increase of RTS fibre content were not compatible. The DIF values of I2.0 and I1.5R0.5 were similar, outperforming other mixtures. The reason why I1.5R0.5 did not surpass I2.0 in terms of DIF can be ascribed to its better internal quality caused by the superior fibre bridging effect, showing a good agreement with previous studies [31, 75]. It was reported that the DIF of concrete tends to be greater when its quality is lower [76], while such conclusion is not valid for the current study. As indicated in the results of quasi-static mechanical properties, UHPC with a large number of RTS fibres may have lower quality and should possess a greater DIF compared to UHPC with fewer RTS fibres. Nevertheless, the DIF values of I0.5R1.5 and R2.0 were still around 1-6% and 6-10% smaller than that of I2.0, implying that further research is required to elucidate this phenomenon.

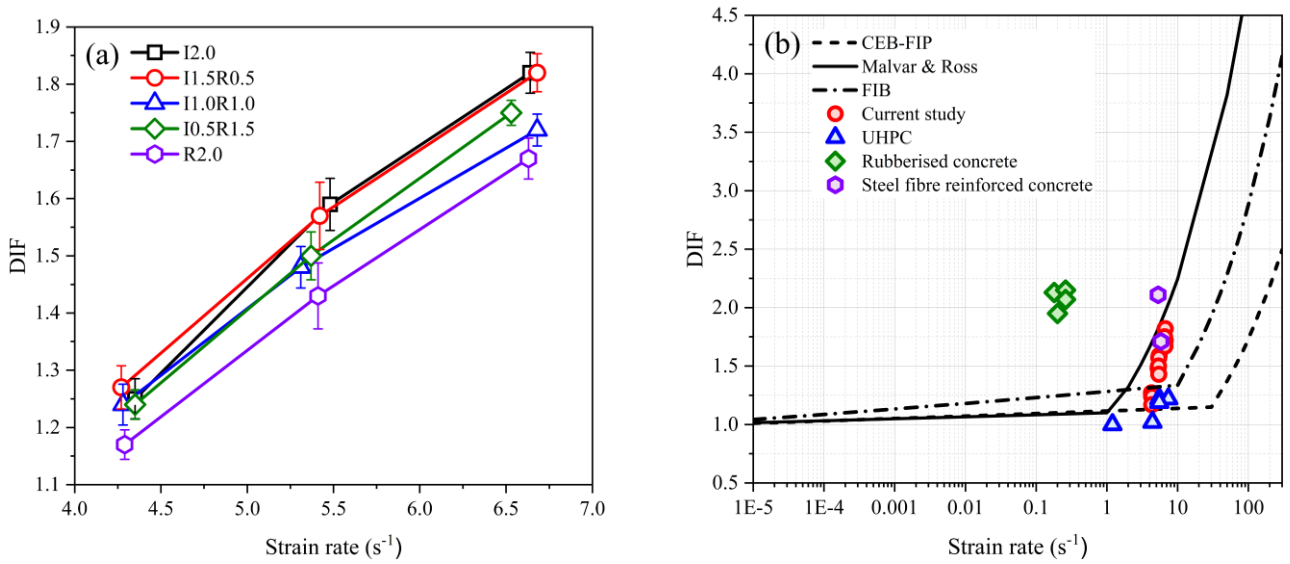

Fig. 18. (a) DIF of UHPC at various strain rates, (b) comparison of DIF gained from the present work with existing models and studies [34, 57, 71, 77-79].

Fig. 18b compares the obtained DIF results in this study with the predicted results using the existing DIF models for normal concrete and literature data. The commonly used DIF models for normal concrete included CEB-FIP model [77], Malvar-Ross model [34] and FIB model [78], which can be expressed as follows:

$$\begin{cases} DIF_{CEB-FIP} = (\frac{\dot{\varepsilon}}{\dot{\varepsilon}_1})^{1.016\alpha} \ \ for\ \dot{\varepsilon} \le 30\ s^{-1} \\ DIF_{CEB-FIP} = \gamma(\frac{\dot{\varepsilon}}{\dot{\varepsilon}_1})^{\frac{1}{3}} \ \ for\ \dot{\varepsilon} > 30\ s^{-1} \end{cases} \quad (4)$$

where $\dot{\varepsilon}_1$ is equal to 0.000003 s^{-1}, α is $(10 + 6\frac{f_c}{f_{c1}})^{-1}$, γ is $10^{(7.11\alpha - 2.33)}$, f_c denotes the quasi-static compressive strength, and f_{c1} = 10 MPa.

$$\begin{cases} DIF_{Malvar-Ross} = (\frac{\dot{\varepsilon}}{\dot{\varepsilon}_2})^{\alpha_1} \ \ for\ \dot{\varepsilon} \le 1\ s^{-1} \\ DIF_{Malvar-Ross} = \gamma_1(\frac{\dot{\varepsilon}}{\dot{\varepsilon}_2})^{\frac{1}{3}} \ \ for\ \dot{\varepsilon} > 1\ s^{-1} \end{cases} \quad (5)$$

where $\dot{\varepsilon}_2$ is equal to 0.000001 s^{-1}, α_1 is $(1 + 8\frac{f_c}{f_{c1}})^{-1}$, and γ_1 is $10^{(6\alpha_1 - 2)}$.

$$\begin{cases} DIF_{FIB} = (\frac{\dot{\varepsilon}}{\dot{\varepsilon}_3})^{0.018} \ \ for\ \dot{\varepsilon} \le 10\ s^{-1} \\ DIF_{FIB} = 0.0062(\frac{\dot{\varepsilon}}{\dot{\varepsilon}_3})^{\frac{1}{3}} \ \ for\ \dot{\varepsilon} > 10\ s^{-1} \end{cases} \quad (6)$$

where $\dot{\varepsilon}_3$ is equal to 0.000001 s^{-1}.

The current DIF results especially at higher strain rates deviated from that predicted using the CEB-FIP and FIB models, which can be ascribed to the unreliability of the CEB-FIP model at high strain rates [34] and the ignorance of quasi-static compressive strength of FIB model (see Eq. (6)). The predicted DIF using the Malvar-Ross model was close to the results of UHPC mixtures with fewer RTS fibres. The compressive and tensile strengths of rubber concrete were 17.91 MPa and 2.21 MPa, respectively, while its DIF ranged from 1.95 to 2.15 at a strain rate of about 0.2 s^{-1} [57]. By contrast, the mixtures containing steel fibres had lower DIF [71, 79]. Under a similar strain rate, the DIF of normal steel fibre reinforced concrete was higher than that of UHPC, showing a good agreement with the discussion above.

3.4.5. Energy absorption capacity

The energy carried by the stress wave typically includes both the elastic strain energy and kinetic energy [58]. Based on the energy conservation law, the energy absorption of UHPC can be determined using Eq. (3). Fig. 19 presents the energy absorption capacity of UHPC under dynamic splitting tensile loading. Regardless of reinforcing fibre, rising the strain rate substantially improved the energy absorption capacity of UHPC specimens, which agrees well with the results of dynamic splitting tensile strength and DIF. For instance, the energy absorption capacity of I1.5R0.5 was increased by 18.12% and 48.32% with the increase of strain rate from 4.27 s^{-1} to 5.42 s^{-1} and 6.68 s^{-1}, respectively, which can be mainly attributed to the rapid propagation of major splitting cracks and the appearance of more micro-cracks [51, 56].

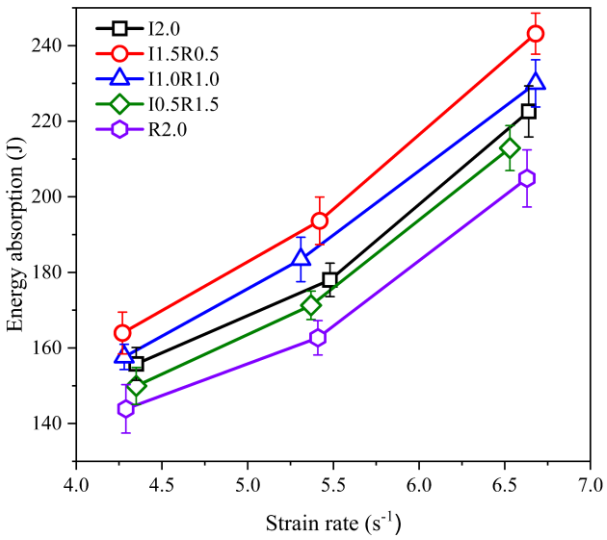

Fig. 19. Relationship between energy absorption and strain rate for all UHPC mixtures.

Additional energy is required for UHPC to pull out or rupture the steel fibres, leading to a higher energy absorption capacity of UHPC than plain mortar. The changing trend of energy absorption with the increase of RTS fibre content was consistent with that of quasi-static mechanical properties and dynamic splitting tensile strength. Replacing IS fibre with 0.5% and 1.0% RTS fibre resulted in a 1.19-9.25% higher energy absorption capacity compared to UHPC with 2.0% IS fibre, while UHPC containing an excessive dosage of RTS fibre absorbed less energy. To better interpret the results above, the fibre distribution of some UHPC specimens at the cracking interfaces is shown in Fig. 20. Many long pulled out steel fibres can be observed for I2.0 and I1.5R0.5 and the complete fibre pull-out is beneficial for the improved energy absorption. The fibre distribution of I1.5R0.5 seemed to be more uniform compared to that of I2.0, which greatly contributed to the enhancement of energy absorption. Fewer IS fibres and more deformed RTS fibres can be observed at the crack interface of I1.0R1.0. Although rising the RTS fibre dosage over a certain content would weaken the energy absorption capacity of UHPC, the improved bonding between deformed RTS fibre and matrix can still increase the friction during the pull-out process and thereby absorbing more energy. Such competition effect led to a comparable energy absorption capacity of I1.0R1.0 to that of I2.0. Previous studies reported that replacing long straight IS fibres with short straight IS fibres did not benefit the energy absorption capacity of UHPC under dynamic compression, drop hammer impact and Charpy impact tests, indicating the dominant effect of long IS fibre in terms of the energy absorption capacity [30, 64, 67]. While in this study, replacing long straight IS fibres with a certain dosage of deformed RTS fibres can improve the energy absorption capacity of UHPC under various strain rates, primarily owing to the interfacial behaviour between RTS fibres and the matrix.

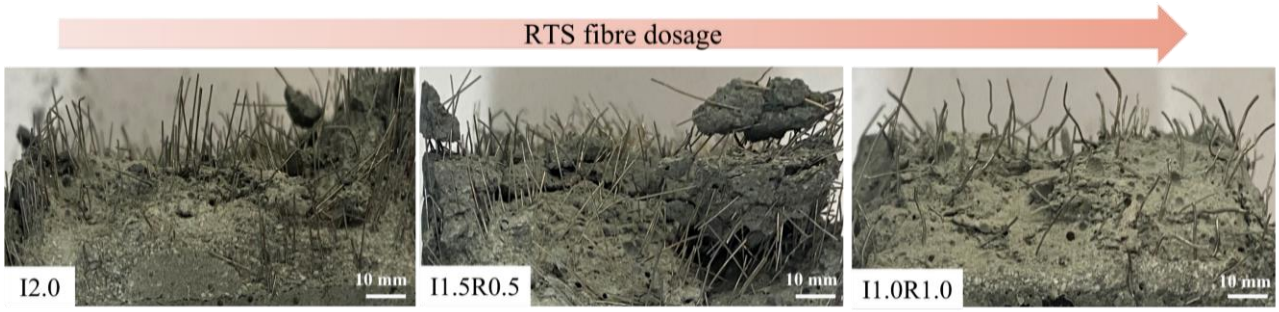

Fig. 20. Fibre distribution of UHPC at the cracking interface after dynamic loading.

3.5. Material cost and environmental impact

To assess the cost-effectiveness and environmental impact of UHPC with RTS fibres, the material cost, embodied carbon and embodied energy per m^3 of all UHPC mixtures were calculated based on the data of each ingredient given in Table 4 and Fig. 21. It is worth noting that the calculated material cost here was employed to briefly reveal the potential economic benefit of using RTS fibres to substitute IS fibres in UHPC, while the actual material cost may vary as the price of each ingredient can change with regions, manufacturers and producing years. The material cost of I2.0 was about 684 USD/m^3, which was 16.77-135.00% higher than that of UHPC containing RTS fibres (Fig. 21a). Similar trends were found for embodied carbon and energy (Figs. 21b and c), where R2.0 exhibited the lowest values of around 730 kg CO_2.eq/m^3 and 6050 MJ/m^3, respectively.

Fig. 22 compares the static and dynamic mechanical performance as well as total material cost and environmental impact between UHPC incorporating solely IS fibres and hybrid fibre reinforced UHPC. In general, apart from the reduced material cost and environmental impact, the workability of UHPC with IS fibres only can be improved by adding RTS fibres. Replacing IS fibres with RTS fibres up to 1.0% fibre content is beneficial for the compressive strength, flexural strength, tensile strength and dynamic mechanical properties of UHPC, implying that 1.0% is the limit for the IS fibre replacement. The most cost-effective mixture was I1.5R0.5 as it can not only achieve better workability, compressive strength and sustainability than I2.0, but also exhibit a 7.33% higher flexural strength, an 8.99-11.86% higher tensile strength, a 10.89-13.60% higher dynamic splitting tensile strength, and a 5.24-9.25% higher dynamic energy absorption capacity.

Table 4 Estimated material cost and life cycle inventory data of each ingredient for UHPC [8, 80-86].

Material type	Cost (USD/kg)	Embodied carbon (kg CO_2.eq/kg)	Embodied energy (MJ/kg)
Cement	0.072	0.83	4.6
Silica fume	0.12	0.014	0.1
Quartz sand	0.025	0.025	0.17
Superplasticiser	1.21	1.5	35
IS fibre	3.53	2.68	35.3
RTS fibre	1.01	0.083	9.5

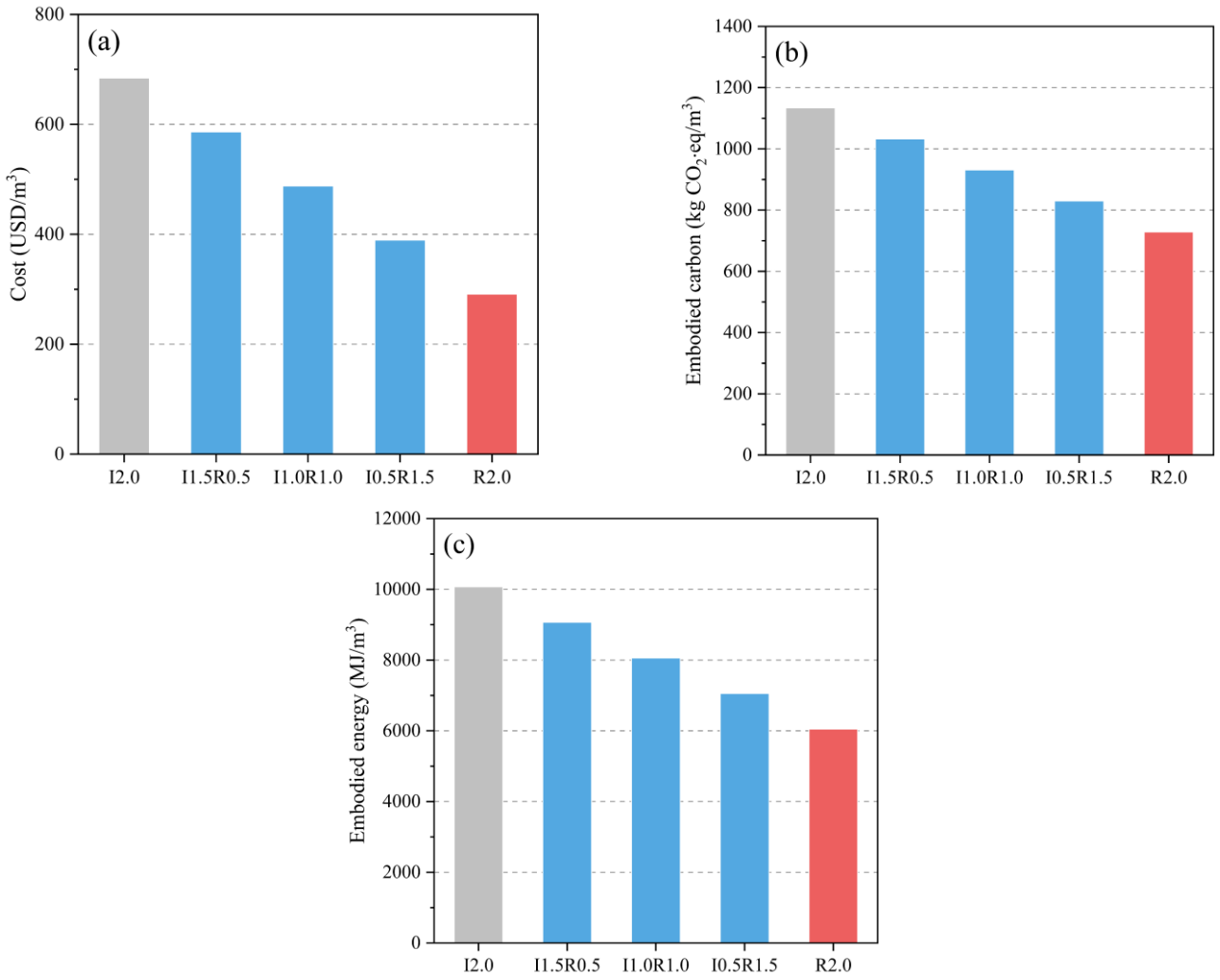

Fig. 21. (a) Material cost, (b) embodied carbon, and (c) embodied energy of all UHPC mixtures.

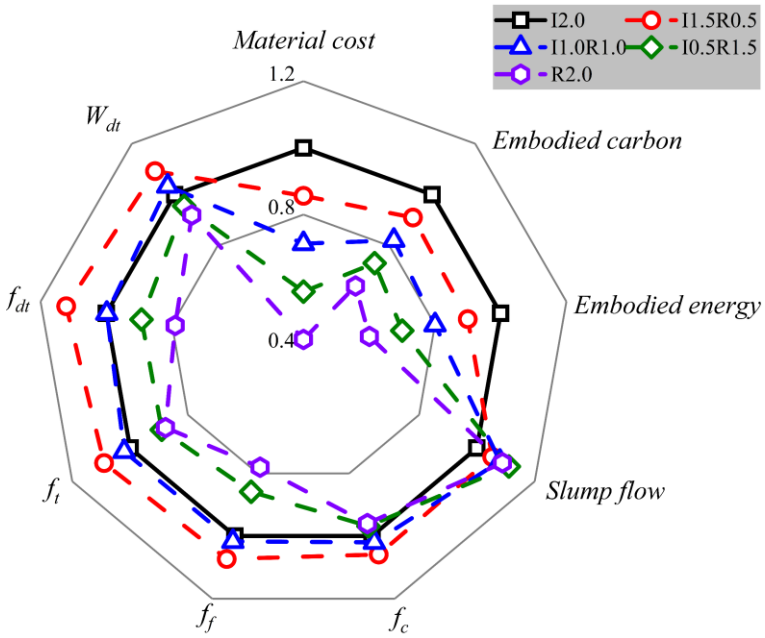

Fig. 22. A comparison between mono-fibre and hybrid fibre reinforced UHPC (f_t = uniaxial tensile strength, f_c = compressive strength, f_f = flexural strength, f_{dt} = dynamic splitting tensile strength, W_{dt} = energy absorption capacity under dynamic splitting tension).

4. Conclusions

In this study, the effect of partially or fully replacing industrial steel (IS) fibres with recycled tyre steel (RTS) fibres (0.5-2.0% fibre volume fraction) on the workability, quasi-static mechanical properties and dynamic splitting tensile properties of ultra-high performance concrete (UHPC) was experimentally investigated. Based on the results obtained, the following conclusions can be drawn:

- Compared to UHPC with 2.0% IS fibre, the addition of RTS fibres enhanced the workability by about 5-11% and the quasi-static compressive, flexural and tensile strengths of UHPC with no more than 1.0% RTS fibre were 2-12% greater.
- There existed a pronounced strain rate dependency for the dynamic splitting tensile behaviour of all studied UHPC specimens, whose damage degree, dynamic splitting tensile strength, dynamic increase factor (DIF), and energy absorption capacity went up with the increasing strain rate.
- Given the better synergistic effect of IS and RTS fibres in limiting the cracks, UHPC reinforced with hybrid 1.5% IS fibre and 0.5% RTS fibre achieved the highest dynamic splitting tensile strength and energy absorption capacity under various strain rates, in comparison with other mixtures. The excessive usage of RTS fibres (over 1.0%) in UHPC induced lower dynamic mechanical properties compared to UHPC with 2.0% IS fibre.
- The changing trend of DIF with RTS fibre replacement level was not consistent with that of quasi-static and other dynamic properties. The measured DIF values of UHPC containing fewer RTS fibres were close to the predictions by the Malvar-Ross model.
- Replacing IS fibres with RTS fibres reduced the material cost, embodied carbon and embodied energy of mono-fibre reinforced UHPC by around 9-57%. UHPC with 1.5% IS fibre and 0.5% RTS fibre can be regarded as the most cost-effective mix, which achieved 11-14% and 5-9% higher dynamic splitting tensile strength and energy absorption capacity than the reference UHPC with 2.0% IS fibre as well as acceptable workability, superior quasi-static mechanical properties, and higher sustainability.

The aforementioned results suggest that utilising 0.5-1.0% RTS fibre to replace IS fibre in UHPC can improve its quasi-static and dynamic mechanical properties as well as reduce the material cost and environmental impact. However, UHPC is vulnerable to damage induced by high temperatures due to its dense microstructure [87]. Towards practical applications, the effect of RTS fibre content on the engineering properties of IS fibre reinforced UHPC at elevated temperatures needs to be studied in depth, which is the subject of ongoing research and will be presented in future publications.

Acknowledgements

This research was funded by the National Natural Science Foundation of China (No. 52178382), the Fundamental Research Funds for the Central Universities (No. N2201023) and the Natural Science Funds of Liaoning Province (No. 2020-MS-089). M. Zhang gratefully acknowledges the financial

support from the Engineering and Physical Sciences Research Council (EPSRC) under Grant No. EP/R041504/1 and the Royal Society under Award No. IEC\NSFC\191417.

References

[1] J. Du, W. Meng, K.H. Khayat, Y. Bao, P. Guo, Z. Lyu, A. Abu-obeidah, H. Nassif, H. Wang, New development of ultra-high-performance concrete (UHPC), Composites Part B: Engineering 224 (2021) 109220.

[2] C. Shi, Z. Wu, J. Xiao, D. Wang, Z. Huang, Z. Fang, A review on ultra high performance concrete: Part I. Raw materials and mixture design, Construction and Building Materials 101 (2015) 741-751.

[3] Q. Meng, C. Wu, J. Li, Z. Liu, P. Wu, Y. Yang, Z. Wang, Steel/basalt rebar reinforced Ultra-High Performance Concrete components against methane-air explosion loads, Composites Part B: Engineering 198 (2020) 108215.

[4] B. Graybeal, E. Brühwiler, B.-S. Kim, F. Toutlemonde, Y.L. Voo, A. Zaghi, International Perspective on UHPC in Bridge Engineering, 25(11) (2020) 04020094.

[5] X. Hou, S. Cao, W. Zheng, Q. Rong, G. Li, Experimental study on dynamic compressive properties of fiber-reinforced reactive powder concrete at high strain rates, Engineering Structures 169 (2018) 119-130.

[6] M. Abo El-Khier, G. Morcous, Precast concrete deck-to-girder connection using Ultra-High Performance Concrete (UHPC) shear pockets, Engineering Structures 248 (2021) 113082.

[7] B.A. Graybeal, Development of Non-Proprietary Ultra-High Performance Concrete for Use in the Highway Bridge Sector: TechBrief, United States. Federal Highway Administration, 2013.

[8] M.N. Isa, K. Pilakoutas, M. Guadagnini, H. Angelakopoulos, Mechanical performance of affordable and eco-efficient ultra-high performance concrete (UHPC) containing recycled tyre steel fibres, Construction and Building Materials 255 (2020) 119272.

[9] G. Malarvizhi, N. Senthul, C. Kamaraj, A study on Recycling of crumb rubber and low density polyethylene blend on stone matrix asphalt, International Journal of Science and Research 2(10) (2012) 1-16.

[10] B.S. Thomas, R.C. Gupta, A comprehensive review on the applications of waste tire rubber in cement concrete, Renewable and Sustainable Energy Reviews 54 (2016) 1323-1333.

[11] S. Gigli, D. Landi, M. Germani, Cost-benefit analysis of a circular economy project: a study on a recycling system for end-of-life tyres, Journal of Cleaner Production 229 (2019) 680-694.

[12] K.M. Liew, A. Akbar, The recent progress of recycled steel fiber reinforced concrete, Construction and Building Materials 232 (2020) 117232.

[13] M. Chen, H. Si, X. Fan, Y. Xuan, M. Zhang, Dynamic compressive behaviour of recycled tyre steel fibre reinforced concrete, Construction and Building Materials 316 (2022) 125896.

[14] B. Ali, R. Kurda, H. Ahmed, R. Alyousef, Effect of recycled tyre steel fiber on flexural toughness, residual strength, and chloride permeability of high-performance concrete (HPC), Journal of Sustainable Cement-Based Materials (2022) 1-17.
[15] Ł. Skarżyński, J. Suchorzewski, Mechanical and fracture properties of concrete reinforced with recycled and industrial steel fibers using Digital Image Correlation technique and X-ray micro computed tomography, Construction and Building Materials 183 (2018) 283-299.
[16] M. Leone, G. Centonze, D. Colonna, F. Micelli, M.A. Aiello, Fiber-reinforced concrete with low content of recycled steel fiber: Shear behaviour, Construction and Building Materials 161 (2018) 141-155.
[17] G. Centonze, M. Leone, M.A. Aiello, Steel fibers from waste tires as reinforcement in concrete: A mechanical characterization, Construction and Building Materials 36 (2012) 46-57.
[18] M.A. Aiello, F. Leuzzi, G. Centonze, A. Maffezzoli, Use of steel fibres recovered from waste tyres as reinforcement in concrete: pull-out behaviour, compressive and flexural strength, Waste Manag 29(6) (2009) 1960-70.
[19] A. Caggiano, P. Folino, C. Lima, E. Martinelli, M. Pepe, On the mechanical response of Hybrid Fiber Reinforced Concrete with Recycled and Industrial Steel Fibers, Construction and Building Materials 147 (2017) 286-295.
[20] D. Bjegovic, A. Baricevic, S. Lakusic, D. Damjanovic, I. Duvnjak, Positive Interaction of Industrial and Recycled Steel Fibres in Fibre Reinforced Concrete, Journal of Civil Engineering and Management 19 (2014) S50-S60.
[21] H. Hu, P. Papastergiou, H. Angelakopoulos, M. Guadagnini, K. Pilakoutas, Mechanical properties of SFRC using blended manufactured and recycled tyre steel fibres, Construction and Building Materials 163 (2018) 376-389.
[22] E. Martinelli, A. Caggiano, H. Xargay, An experimental study on the post-cracking behaviour of Hybrid Industrial/Recycled Steel Fibre-Reinforced Concrete, Construction and Building Materials 94 (2015) 290-298.
[23] M. Mastali, A. Dalvand, A.R. Sattarifard, Z. Abdollahnejad, M. Illikainen, Characterization and optimization of hardened properties of self-consolidating concrete incorporating recycled steel, industrial steel, polypropylene and hybrid fibers, Composites Part B: Engineering 151 (2018) 186-200.
[24] M. Mastali, A. Dalvand, A.R. Sattarifard, M. Illikainen, Development of eco-efficient and cost-effective reinforced self-consolidation concretes with hybrid industrial/recycled steel fibers, Construction and Building Materials 166 (2018) 214-226.

[25] O. Onuaguluchi, N. Banthia, Scrap tire steel fiber as a substitute for commercial steel fiber in cement mortar: Engineering properties and cost-benefit analyses, Resources, Conservation and Recycling 134 (2018) 248-256.
[26] M.N. Isa, K. Pilakoutas, M. Guadagnini, Shear behaviour of E-UHPC containing recycled steel fibres and design of E-UHPC screw piles, Construction and Building Materials 304 (2021) 124555.
[27] M.N. Isa, K. Pilakoutas, M. Guadagnini, Determination of tensile characteristics and design of eco-efficient UHPC, Structures 32 (2021) 2174-2194.
[28] H. Abdolpour, P. Niewiadomski, Ł. Sadowski, A. Kwiecień, Engineering of ultra-high performance self-compacting mortar with recycled steel fibres extracted from waste tires, Archives of Civil and Mechanical Engineering 22(4) (2022) 175.
[29] Y.Y.Y. Cao, Q.L. Yu, H.J.H. Brouwers, W. Chen, Predicting the rate effects on hooked-end fiber pullout performance from Ultra-High Performance Concrete (UHPC), Cement and Concrete Research 120 (2019) 164-175.
[30] Z. Wu, C. Shi, W. He, D. Wang, Static and dynamic compressive properties of ultra-high performance concrete (UHPC) with hybrid steel fiber reinforcements, Cement and Concrete Composites 79 (2017) 148-157.
[31] J. Lai, W. Sun, Dynamic behaviour and visco-elastic damage model of ultra-high performance cementitious composite, Cement and Concrete Research 39(11) (2009) 1044-1051.
[32] Q. Yu, W. Zhuang, C. Shi, Research progress on the dynamic compressive properties of ultra-high performance concrete under high strain rates, Cement and Concrete Composites 124 (2021) 104258.
[33] M. Hassan, K. Wille, Experimental impact analysis on ultra-high performance concrete (UHPC) for achieving stress equilibrium (SE) and constant strain rate (CSR) in Split Hopkinson pressure bar (SHPB) using pulse shaping technique, Construction and Building Materials 144 (2017) 747-757.
[34] L.J. Malvar, C.A. Ross, Review of strain rate effects for concrete in tension, ACI Mater. J. 95 (1998) 735-739.
[35] D.-Y. Yoo, N. Banthia, Impact resistance of fiber-reinforced concrete – A review, Cement and Concrete Composites 104 (2019) 103389.
[36] M.R. Khosravani, Inverse characterization of UHPC material based on Hopkinson bar test, Applications in Engineering Science 6 (2021) 100043.
[37] K. Fujikake, T. Senga, N. Ueda, T. Ohno, M. Katagiri, Effects of strain rate on tensile behavior of reactive powder concrete, Journal of Advanced Concrete Technology 4(1) (2006) 79-84.
[38] Y. Su, J. Li, C. Wu, P. Wu, Z.-X. Li, Influences of nano-particles on dynamic strength of ultra-high performance concrete, Composites Part B: Engineering 91 (2016) 595-609.

[39] H. Wu, G.M. Ren, Q. Fang, J.Z. Liu, Effects of steel fiber content and type on dynamic tensile mechanical properties of UHPCC, Construction and Building Materials 173 (2018) 251-261.
[40] E. Cadoni, D. Forni, E. Bonnet, S. Dobrusky, Experimental study on direct tensile behaviour of UHPFRC under high strain-rates, Construction and Building Materials 218 (2019) 667-680.
[41] M. Hassan, K. Wille, Direct tensile behavior of steel fiber reinforced ultra-high performance concrete at high strain rates using modified split Hopkinson tension bar, Composites Part B: Engineering 246 (2022) 110259.
[42] S. Gurusideswar, A. Shukla, K.N. Jonnalagadda, P. Nanthagopalan, Tensile strength and failure of ultra-high performance concrete (UHPC) composition over a wide range of strain rates, Construction and Building Materials 258 (2020) 119642.
[43] X. Chen, S. Wu, J. Zhou, Quantification of dynamic tensile behavior of cement-based materials, Construction and Building Materials 51 (2014) 15-23.
[44] H. Zhong, M. Zhang, Dynamic splitting tensile behaviour of engineered geopolymer composites with hybrid polyvinyl alcohol and recycled tyre polymer fibres, Journal of Cleaner Production 379 (2022) 134779.
[45] D. Ravichandran, P.R. Prem, S.K. Kaliyavaradhan, P.S. Ambily, Influence of fibers on fresh and hardened properties of Ultra High Performance Concrete (UHPC)—A review, Journal of Building Engineering 57 (2022) 104922.
[46] J. Feng, W.W. Sun, X.M. Wang, X.Y. Shi, Mechanical analyses of hooked fiber pullout performance in ultra-high-performance concrete, Construction and Building Materials 69 (2014) 403-410.
[47] ASTM C1437-15, Standard Test Method for Flow of Hydraulic Cement Mortar, ASTM International, West Conshohocken, PA, United States, 2015.
[48] EN196-1, Methods of Testing Cement-Part 1: Determination of Strength, British Standards Institution-BSI and CEN European Committee for Standardization, 2005.
[49] Japan Society of Civil Engineers, Recommendations for design and construction of high performance fiber reinforced cement composites with multiple fine cracks (HPFRCC), Concrete Engineering Series No. 82 (2008).
[50] M.Z.N. Khan, Y. Hao, H. Hao, F.u.A. Shaikh, Mechanical properties and behaviour of high-strength plain and hybrid-fiber reinforced geopolymer composites under dynamic splitting tension, Cement and Concrete Composites 104 (2019) 103343.
[51] M. Chen, H. Zhong, H. Wang, M. Zhang, Behaviour of recycled tyre polymer fibre reinforced concrete under dynamic splitting tension, Cement and Concrete Composites 114 (2020) 103764.
[52] ASTM C496, Standard Test Method for Splitting Tensile Strength of Cylindrical Concrete Specimens, ASTM International, West Conshohocken, PA 2017.

[53] M. Chen, W. Chen, H. Zhong, D. Chi, Y. Wang, M. Zhang, Experimental study on dynamic compressive behaviour of recycled tyre polymer fibre reinforced concrete, Cement and Concrete Composites 98 (2019) 95-112.
[54] W. W. Chen, B. Song, Split Hopkinson (Kolsky) Bar: Design, Testing and Applications, Springer2011.
[55] T. Guo, K. Liu, S. Ma, J. Yang, X. Li, K. Zhou, T. Qiu, Dynamic fracture behavior and fracture toughness analysis of rock-concrete bi-material with interface crack at different impact angles, Construction and Building Materials 356 (2022) 129286.
[56] D. Lai, C. Demartino, Y. Xiao, High-strain rate tension behavior of Fiber-Reinforced Rubberized Concrete, Cement and Concrete Composites 131 (2022) 104554.
[57] W. Feng, F. Liu, F. Yang, L. Li, L. Jing, Experimental study on dynamic split tensile properties of rubber concrete, Construction and Building Materials 165 (2018) 675-687.
[58] B. Song, W. Chen, Energy for specimen deformation in a split Hopkinson pressure bar experiment, Experimental mechanics 46(3) (2006) 407-410.
[59] M. Farooq, A. Bhutta, N. Banthia, Tensile performance of eco-friendly ductile geopolymer composites (EDGC) incorporating different micro-fibers, Cement and Concrete Composites 103 (2019) 183-192.
[60] J. Gong, Y. Ma, J. Fu, J. Hu, X. Ouyang, Z. Zhang, H. Wang, Utilization of fibers in ultra-high performance concrete: A review, Composites Part B: Engineering 241 (2022) 109995.
[61] L. Martinie, P. Rossi, N. Roussel, Rheology of fiber reinforced cementitious materials: classification and prediction, Cement and Concrete Research 40(2) (2010) 226-234.
[62] Z. Wu, C. Shi, W. He, L. Wu, Effects of steel fiber content and shape on mechanical properties of ultra high performance concrete, Construction and Building Materials 103 (2016) 8-14.
[63] W. Meng, K.H. Khayat, Effect of hybrid fibers on fresh properties, mechanical properties, and autogenous shrinkage of cost-effective UHPC, J. Mater. Civ. Eng 30(4) (2018) 04018030.
[64] R. Yu, P. Spiesz, H.J.H. Brouwers, Static properties and impact resistance of a green Ultra-High Performance Hybrid Fibre Reinforced Concrete (UHPHFRC): Experiments and modeling, Construction and Building Materials 68 (2014) 158-171.
[65] H. Zhong, M. Zhang, Experimental study on engineering properties of concrete reinforced with hybrid recycled tyre steel and polypropylene fibres, Journal of Cleaner Production 259 (2020) 120914.
[66] R. Shao, C. Wu, J. Li, Z. Liu, Investigation on the mechanical characteristics of multiscale mono/hybrid steel fibre-reinforced dry UHPC, Cement and Concrete Composites 133 (2022) 104681.
[67] J. Wei, J. Li, C. Wu, Z.-x. Liu, J. Li, Hybrid fibre reinforced ultra-high performance concrete beams under static and impact loads, Engineering Structures 245 (2021) 112921.

[68] N. Ranjbar, M. Zhang, Fiber-reinforced geopolymer composites: A review, Cement and Concrete Composites 107 (2020) 103498.
[69] J. Li, J. Weng, Z. Chen, E.-H. Yang, A generic model to determine crack spacing of short and randomly oriented polymeric fiber-reinforced strain-hardening cementitious composites (SHCC), Cement and Concrete Composites 118 (2021) 103919.
[70] H. Zhong, M. Zhang, Engineered geopolymer composites: A state-of-the-art review, Cement and Concrete Composites 135 (2023) 104850.
[71] X. Zhao, Q. Li, S. Xu, Contribution of steel fiber on the dynamic tensile properties of hybrid fiber ultra high toughness cementitious composites using Brazilian test, Construction and Building Materials 246 (2020) 118416.
[72] H. Zhong, M. Zhang, Effect of recycled tyre polymer fibre on engineering properties of sustainable strain hardening geopolymer composites, Cement and Concrete Composites 122 (2021) 104167.
[73] Y. Hao, H. Hao, Mechanical properties and behaviour of concrete reinforced with spiral-shaped steel fibres under dynamic splitting tension, Magazine of Concrete Research 68(21) (2016) 1110-1121.
[74] Y. Hao, H. Hao, G.P. Jiang, Y. Zhou, Experimental confirmation of some factors influencing dynamic concrete compressive strengths in high-speed impact tests, Cement and Concrete Research 52 (2013) 63-70.
[75] G.M. Ren, H. Wu, Q. Fang, J.Z. Liu, Effects of steel fiber content and type on dynamic compressive mechanical properties of UHPCC, Construction and Building Materials 164 (2018) 29-43.
[76] P.H. Bischoff, S.H. Perry, Compressive behaviour of concrete at high strain rates, Materials and Structures 24(6) (1991) 425-450.
[77] CEB-FIP model code 1990: Design code, Comite Euro-Inernational Du Beton 1990.
[78] FIB Model Code for Concrete Structures 2010, Comite Euro-Inernational Du Beton 2013.
[79] X. Zhao, B. Zou, M. Wang, H. Li, Z. Lou, Influence of free water on dynamic tensile behavior of ultra-high toughness cementitious composites, Construction and Building Materials 269 (2021) 121295.
[80] G. Hammond, C. Jones, F. Lowrie, P. Tse, Inventory of carbon & energy: ICE, Sustainable Energy Research Team, Department of Mechanical Engineering 2008.
[81] R. Sharma, R.A. Khan, Sustainable use of copper slag in self compacting concrete containing supplementary cementitious materials, Journal of Cleaner Production 151 (2017) 179-192.

[82] D. Zhang, B. Jaworska, H. Zhu, K. Dahlquist, V.C. Li, Engineered Cementitious Composites (ECC) with limestone calcined clay cement (LC3), Cement and Concrete Composites 114 (2020) 103766.
[83] R. Ranade, Advanced cementitious composite development for resilient and sustainable infrastructure, University of Michigan, 2014.
[84] G.A. Keoleian, A. Kendall, J.E. Dettling, V.M. Smith, R.F. Chandler, M.D. Lepech, V.C. Li, Life cycle modeling of concrete bridge design: Comparison of engineered cementitious composite link slabs and conventional steel expansion joints, J. Infrastruct. Syst. 11 (2005) 51-60.
[85] G. Habert, E. Denarié, A. Šajna, P. Rossi, Lowering the global warming impact of bridge rehabilitations by using Ultra High Performance Fibre Reinforced Concretes, Cement and Concrete Composites 38 (2013) 1-11.
[86] Z.-h. He, H.-n. Zhu, M.-y. Zhang, J.-y. Shi, S.-g. Du, B. Liu, Autogenous shrinkage and nano-mechanical properties of UHPC containing waste brick powder derived from construction and demolition waste, Construction and Building Materials 306 (2021) 124869.
[87] Y. Zhu, H. Hussein, A. Kumar, G. Chen, A review: Material and structural properties of UHPC at elevated temperatures or fire conditions, Cement and Concrete Composites 123 (2021) 104212.